Accuracy of RGD approximation for computing light scattering properties of diffusing and motile bacteria

Michael Kotlarchyk, Sow-Hsin Chen, and Shoji Asano

The quasi-elastic light scattering has become an established technique for a rapid and quantitative characterization of an average motility pattern of motile bacteria in suspensions. Essentially all interpretations of the measured light scattering intensities and spectra so far are based on the Rayleigh-Gans-Debye (RGD) approximation. Since the range of sizes of bacteria of interest is generally larger than the wavelength of light used in the measurement, one is not certain of the justification for the use of the RGD approximation. In this paper we formulate a method by which both the scattering intensity and the quasi-elastic light scattering spectra can be calculated from a rigorous scattering theory. For a specific application we study the case of bacteria *Escherichia coli* (about 1 μm in size) by using numerical solutions of the scattering field amplitudes from a prolate spheroid, which is known to simulate optical properties of the bacteria well. We have computed (1) polarized scattered light intensity vs scattering angle for a randomly oriented bacteria population; (2) polarized scattered field correlation functions for both a freely diffusing bacterium and for a bacterium undergoing a straight line motion in random directions and with a Maxwellian speed distribution; and (3) the corresponding depolarized scattered intensity and field correlation functions. In each case sensitivity of the result to variations of the index of refraction and size of the bacterium is investigated. The conclusion is that within a reasonable range of parameters applicable to *E. coli*, the accuracy of the RGD is good to within 10% at all angles for the properties (1) and (2), and the depolarized contributions in (3) are generally very small.

I. Introduction

Light scattering intensity measurements from small particles suspended in fluids have long been used for characterization of sizes and shapes of the particles.[1,2] A natural application of this technique is to use it for the size assay of bacteria in liquid suspension.[3] In 1971 Nossal *et al.*[4] demonstrated that the quasi-elastic light scattering spectrum, or equivalently the time correlation function of the scattered field amplitude, depends sensitively on the speed distribution of a collection of motile bacteria homogeneously suspended in liquid media. Since then many workers have used this technique to study various motility characteristics of bacteria and microorganisms under different controls.[5]

Recently, in a series of articles[6–8] we undertook to systematically analyze theoretically and test experimentally the effects of finite size, shape, and structure of a specific model bacteria *Escherichia coli* on the measured angular dependence of polarized scattered intensity and also on the field amplitude correlation function. The basic scattering amplitude from a finite size particle was computed in the RGD approximation in Ref. 6 and used to predict the measured intensity distribution and the angular dependence of the correlation function. We modeled the *E. coli* bacterium as a coated prolate spheroid of semimajor and minor axes a and b, having a cell wall thickness t. In Ref. 7 we showed that this model of *E. coli* reproduces most of the light scattering properties well with a reasonable choice of a set of parameters, except that the angular dependence of the halfwidth of the correlation function cannot be accounted for by assuming a simple straight line translation of the bacteria in random direction. We therefore in Ref. 8 extended our calculation to take into account possible translation-rotational motions of the spheroid. We showed there that a large part of the discrepancy in the halfwidth of the correlation function at large angle can be attributed to superposition of a helical motion of *E. coli* around the direction of the translation. A further refinement of the model of motion taking into account sequential "run" and "twiddle" motions was presented in Ref. 9.

Results of these studies[6–9] show that in treating the light scattering data of micron size particles the finite

Shoji Asano is with Goddard Institute for Space Studies, New York, New York 10025. The first two authors named were with Massachusetts Institute of Technology, Nuclear Engineering Department, Cambridge, Massachusetts 02139; M. Kotlarchyk is now with Polaroid Corporation, Equipment & Facility Engineering, Waltham, Massachusetts 02154.

Received 11 January 1979.
0003-6935/79/142470-10$00.50/0.

size, shape, and structural effects play an important role, besides the more obvious dependence on the modes of motion of particles themselves. It was shown[6] that using the RGD approximation these finite size, shape, and structural effects can be incorporated into the intensity and correlation function calculations quite straightforwardly. However, the RGD approximation is valid only in the limit of small size and small index of refraction difference between the particle and the surrounding medium. More specifically it is valid when[1,2]

$$|m-1| \ll 1, \tag{1}$$

$$kd|m-1| \ll 1, \tag{2}$$

where $m \equiv n/n_0$ is the ratio of index of refraction of the particle to that of the surrounding medium, d is the characteristic dimension of the particle, and $k = 2\pi/\lambda$, where λ is the wavelength of light in the medium. For *E. coli* our previous study[7] shows that the intensity distribution data are consistent with a choice of the spheroid parameters $a = 0.70$ μm, $b = 0.36$ μm, and index of refraction of the particle $n = 1.342$. Taking the medium to be water with $n_0 = 1.333$ we have $m - 1 = 0.007$, which is indeed small. But $2ka|m-1| = 0.154$, which is not obviously small enough. On the other hand if we take a literative value[3] of $n = 1.370$, then $m - 1 = 0.03$ and $2ka|m-1| = 0.68$. In this latter case there is some doubt as to whether the RGD approximation is useful.

Under this circumstance it is desirable to be able to establish at least the range of errors one could expect in consistently using the RGD approximation for calculations of light scattering properties of a microorganism. This estimate is possible only when a calculation can be made based on a rigorous scattering theory for the given particle geometry. Fortunately a numerical solution of the scattering amplitude from a spheroid is now available.[10] We can therefore test the accuracy of the RGD approximation against this rigorous scattering theory calculation for a simplified model of *E. coli*—a solid spheroid.

In Sec. II we formulate a general procedure by which the scattered field amplitude correlation function can be calculated for a particle situated at an arbitrary position $\overline{R}(t)$ from the solution for a particle situated at the origin. At time zero this correlation function gives the intensity distribution, and at finite time it gives the desired time correlation function. For computing quantities of interest in experiments a laboratory coordinate system has to be used which is not the body fix coordinate system convenient for the solution of the boundary value problem. Therefore, a coordinate transformation between the two coordinate systems is described. In Sec. III we briefly describe the computer code which is used for the correlation function calculations. In Sec. IV we discuss the results in terms of the intensity distribution, the correlation function for a diffusing spheroid, and the correlation function for a spheroid moving in a straight line in random directions with a Maxwellian speed distribution and then discuss the depolarized contributions. We conclude in Sec. V with an assessment of accuracy of the RGD approximation in the case of *E. coli* and some remarks on interpretation of quasi-elastic light scattering spectra of other microorganisms. To our knowledge, this work seems to be the first treatment of the quasi-elastic light spectra in terms of a rigorous scattering theory.

II. Light Scattering Theory

A complete solution to the problem of scattering of light[1,2] by a homogeneous nonmagnetic particle of index of refraction n (called region I) immersed in a homogeneous dielectric medium of index of refraction n_0 (called region II) can be obtained from the Maxwell's equations

$$\overline{\nabla} \times \overline{E} = ik_v \overline{B}, \tag{3}$$

$$\overline{\nabla} \times \overline{B} = -ik_v n^2(\overline{r})\overline{E}, \tag{4}$$

in regions I and II with the following boundary conditions:

(a) in region I, where $n(\overline{r}) \equiv n$, there are the internal fields $(\overline{E}_i, \overline{B}_i)$;

(b) in region II, where $n(\overline{r}) \equiv n_0$, there are the scattered fields $(\overline{E}_s, \overline{B}_s)$ plus the incident fields

$$\overline{E}_0(\overline{r},t) = E_0\hat{\epsilon} \exp[i(\overline{k}\cdot\overline{r} - \omega t)] \tag{5}$$

and its magnetic counterpart;

(c) the tangential components of the fields in I and II are continuous at the boundary between the particle and the medium.

We use notations $k_v = \omega/c$, wavenumber in vacuum; and $k = n_0 k_v$, wavenumber in the medium; and $\hat{\epsilon}$ the incident field polarization vector.

Figure 1 illustrates a typical scattering geometry. The incident wave vector $\hat{k}$ is in the $\hat{y}$ direction with the polarization vector $\hat{\epsilon}$ along the $\hat{z}$ direction. The scattered wave vector $\hat{k}'$ is taken to be in the $x - y$ plane with a scattering angle Θ. A unit vector $\hat{v}$ denotes the symmetry axis of the particle with its direction specified

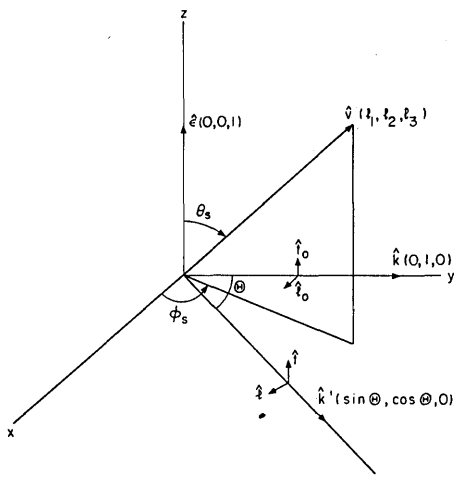

Fig. 1. Laboratory coordinate system showing the directions of incident and scattered waves with their respective polarization vectors. $\hat{V}$ is a unit vector specifying the orientation of the ellipsoid.

by angles (θ_s, ϕ_s). In a most general case involving an arbitrary incident polarization, one can decompose the incident field into a transverse component (perpendicular to the scattering plane) and a parallel component (parallel to the scattering plane), each specified by a unit vector $\hat{t}_0$ and $\hat{l}_0$, respectively. The scattered fields are then also decomposable into transverse and parallel components each specified by a unit vector $\hat{t}$ and $\hat{l}$. Since the Maxwell's equations are linear we have in general a linear relation between the incident and the scattered electric fields[2]

$$\begin{pmatrix} E_{st} \\ E_{sl} \end{pmatrix} = \begin{pmatrix} S_1 S_4 \\ S_3 S_2 \end{pmatrix} \begin{pmatrix} E_{0t} \\ E_{0l} \end{pmatrix} \frac{\exp(ikr)}{-ikr} \exp(-i\bar{k}\cdot\bar{r}), \tag{6}$$

where the elements of the scattering matrix S_i are dimensionless scattering amplitudes which depend on relative orientations of the four vectors: $\hat{v}$, $\hat{\epsilon}$, $\hat{k}$, and $\hat{k}'$. In the usual scattering geometry depicted in Fig. 1, $E_{0l} = 0$, and $E_{0t} = \bar{E}_0(\bar{r},t)$ as given in Eq. (5). The polarized scattered field amplitude is given by S_1, and the depolarized scattered field amplitude is given by S_3. The scattering amplitudes S_i can be determined by solving the Maxwell's equation as a boundary value problem as mentioned above.

A. Integral Formulation of the Scattering Theory and the Rayleigh-Gans-Debye Approximation[6]

The partial differential equation given in Eqs. (3) and (4) can be converted to an integral equation. This can be accomplished by eliminating $\bar{B}$ from Eqs. (3) and (4) to get

$$\bar{\nabla}\times(\bar{\nabla}\times\bar{E}) - k_v^2 n_0^2 \bar{E} = k_v^2[n^2(\bar{r}) - n_0^2]\bar{E}. \tag{7}$$

Equation (7) is then converted into an integral equation by using Green's function $\bar{\bar{G}}$ for the Helmholtz operator on the left-hand side of the equation. Aside from a time factor $\exp(-i\omega t)$ the total field satisfies an integral equation

$$\bar{E}(\bar{r}) = \bar{E}_0(\bar{r}) + \int_v d^3r' \bar{\bar{G}}(\bar{r}-\bar{r}')\cdot k_v^2(n^2 - n_0^2)\bar{E}(\bar{r}'), \tag{8}$$

where the Green's tensor $\bar{\bar{G}}(\bar{r}-\bar{r}')$ is given by

$$\bar{\bar{G}}(\bar{R}) = \left(\bar{\bar{1}} + \frac{1}{k^2}\bar{\nabla}\bar{\nabla}\right)\frac{\exp(ikR)}{4\pi R}, \tag{9}$$

and $R = |\bar{r}-\bar{r}'|$.

In the wave zone where $kR \gg 1$ and $R \gg$ dimension of the particle, the Green's tensor simplifies to

$$\bar{\bar{G}}(R) = (\bar{\bar{1}} - \hat{r}\hat{r})\frac{\exp(ikr - i\bar{k}'\cdot\bar{r}')}{4\pi r}, \tag{10}$$

where $\bar{k}' = k\hat{r}$ is the scattered wave vector.

In Eq. (8), $\bar{E}_0(\bar{r})$ represents the spatial part of the incident field, and therefore the scattered field is given by

$$\bar{E}_s(\bar{r}) = \int_v d^3r' \bar{\bar{G}}(\bar{r}-\bar{r}')\cdot k^2(m^2-1)\bar{E}(\bar{r}'). \tag{11}$$

Notice that the scattered field is completely determined by knowing only the internal field $E_i(\bar{r})$ inside the particle since the integration in Eq. (11) is over the volume of the particle. It is also a function of the relative index of refraction $m = n/n_0$ only.

If the scattering is weak compared with the incident field, $\bar{E}_s(\bar{r})$ can be obtained as an iterated solution

$$\bar{E}_s(\bar{r}) = \sum_{n=1}^{\infty} \bar{E}_n(\bar{r}), \tag{12}$$

where

$$\bar{E}_n(\bar{r}) = k^{2n}(m^2-1)^n \int_v d^3r' \bar{\bar{G}}(\bar{r}-\bar{r}') \cdot \int_v d^3r'' \bar{\bar{G}}(\bar{r}'-\bar{r}'')\cdot \int_v \cdots \cdot \int_v d^3r^{(n)} \bar{\bar{G}}[\bar{r}^{(n-1)} - r^{(n)}]\cdot \bar{E}_0[\bar{r}^{(n)}]. \tag{13}$$

Since all vectors $\bar{r}^{(n)}$ represent points somewhere inside the particle, it is sensible to rewrite them in terms of relative position vectors $\bar{\rho}^{(n)}$ with respect to the center of mass position $\bar{R}$, i.e.,

$$\bar{r}^{(n)} = \bar{R} + \bar{\rho}^{(n)}. \tag{14}$$

We also use the far-field approximation (10) for $\bar{\bar{G}}(\bar{r}-\bar{r}')$ and Eq. (3) for the incident field $\bar{E}_0[r^{(n)}]$ to get

$$\bar{E}_n(\bar{r},t) = A_n(r)\bar{a}_n[\hat{v}(t),\hat{k},\hat{k}',\hat{\epsilon}]\exp[i\bar{q}\cdot\bar{R}(t) - i\omega t], \tag{15}$$

where

$$A_n(r) = E_0 k^{2n}(m^2-1)^n V^n \frac{\exp(ikr)}{4\pi r}, \tag{16}$$

$$\bar{a}_n = \frac{1}{V^n}\int_v d^3\rho'(\bar{\bar{1}} - \hat{r}\hat{r})\exp(-i\bar{k}'\cdot\bar{\rho}') \cdot \int_v d^3\rho'' \bar{\bar{G}}(\bar{\rho}'-\bar{\rho}'')\cdot \int_v \cdots \cdot \int d^3\rho^{(n)} \bar{\bar{G}}(\rho^{(n-1)} - \rho^{(n)})\cdot\hat{\epsilon}\exp[i\bar{k}\cdot\bar{\rho}^{(n)}], \tag{17}$$

and $\bar{q} = \bar{k} - \bar{k}'$ is the scattering vector.

As one can see from Eq. (17) the vector dynamic form factor $\bar{a}_n$ indeed depends on the relative orientation of the four vectors $\hat{v}$, $\hat{k}$, $\hat{k}'$, and $\hat{\epsilon}$. It is also time dependent because orientation of the particle $\hat{v}(t)$ changes in time due to either the rotational diffusion or motion. The RGD approximation amounts to retain only the lowest order $n = 1$ term in the expansion (12). From Eqs. (15), (16), and (17) we have

$$\bar{E}_1(\bar{r},t) = E_0 k^2(m^2-1)V\frac{\exp(ikr)}{4\pi r}\bar{a}_1[\hat{v}(t),\hat{q}]\exp[i\bar{q}\cdot\bar{R}(t) - i\omega t], \tag{18}$$

where the dynamic form factor has a particularly simple form

$$\bar{a}_1[\hat{v}(t),\hat{q}] = (\bar{\bar{1}} - \hat{r}\hat{r})\cdot\hat{\epsilon}\frac{1}{V}\int_v d^3\rho' \exp(i\bar{q}\cdot\bar{\rho}'). \tag{19}$$

$\bar{a}_1$ in the RGD approximation depends only on relative orientation of two vectors $\hat{v}(t)$ and $\hat{q}$. One can see from Eqs. (18) and (19) that in this approximation the time dependence of the scattered field $\bar{E}_1(\bar{r},t)$ comes from two sources: rotational motion of the particle entering through the dynamic form factor $\bar{a}(t)$ and translational motion through the exponential factor $\exp[i\bar{q}\cdot\bar{R}(t) -$

$i\omega t]$. In a typical scattering geometry depicted in Fig. 1, $(\bar{\bar{1}} - \hat{r}\hat{r})\cdot\hat{\epsilon} = \hat{\epsilon}$, and the scattered field is completely polarized. The form factor in Eq. (19) can be evaluated analytically for many symmetric bodies[7] and, in particular, for an ellipsoid of revolution (or a spheroid) with semimajor and minor axes a and b, it is

$$\frac{1}{V}\int d^3\rho' \exp(i\bar{q}\cdot\bar{\rho}) = \frac{3j_1(u)}{u}, \tag{20}$$

where

$$u = q[a^2\mu^2 + b^2(1-\mu^2)]^{1/2}, \tag{21}$$

and $\mu \equiv \hat{q}\cdot\hat{v}$, the cosine of the relative angle between the $\hat{q}$ vector and the symmetry axis of the body.

It is instructive to also write out the second-order term

$$\bar{E}_2(\bar{r},t) = E_0 k^4 (m^2-1)^2 V^2 \frac{\exp(ikr)}{4\pi r}\bar{a}_2(t)\exp[i\bar{q}\cdot\bar{R}(t) - i\omega t], \tag{22}$$

$$\bar{a}_2(t) = \frac{1}{V^2}\int_v d^3\rho'(\bar{\bar{1}} - \hat{r}\hat{r})\exp(-i\bar{k}'\cdot\bar{\rho}') \cdot \int_v d^3\rho''\bar{\bar{G}}(\bar{\rho}' - \bar{\rho}'')\cdot\hat{\epsilon}\exp(i\bar{k}\cdot\bar{\rho}''). \tag{23}$$

We see that already in this order the dynamic form factor $\bar{a}_2(t)$ depends on relative orientation of all four vectors $\hat{v}$, $\hat{k}$, $\hat{k}'$, and $\hat{\epsilon}$. The scattered field is no longer polarized, but contains a depolarized component because of the presence of a tensor $\bar{\bar{G}}(\bar{\rho}' - \bar{\rho}'')$ in Eq. (23). While we can depict the first-order term $\bar{E}_1(\bar{r}_1 t)$ as due to the sum of all single scattering events each occurring at $\bar{\rho}'$ in the body, we can picture the second-order terms $\bar{E}_2(\bar{r}_1 t)$ as due to the sum of all double scattering events occurring at $\bar{\rho}'$ and $\bar{\rho}''$ in the body, as shown in Fig. 2. Two stars in the body represent a typical double scattering event. In fact the nth order term in Eq. (12) can likewise be interpreted as the nth-order multiple scattering contribution to the scattered field. If the series (10) converges, the resultant scattered field should be identical to that calculated by solving the boundary value problem outlined in the beginning of this section.

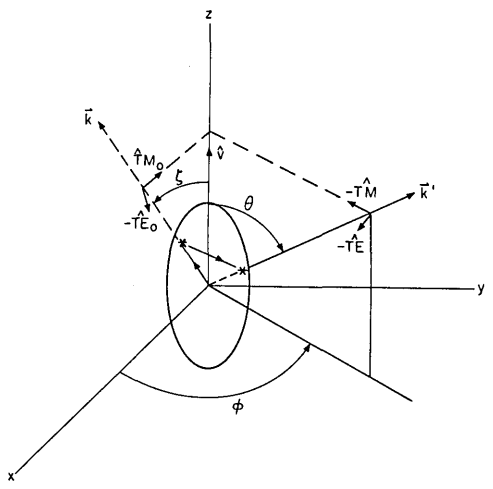

Fig. 2. Coordinate system for the A-Y theory. The ellipsoid is oriented along the z axis. The incident wave vector $\mathbf{k}$ lies in the $\phi = 0°$ plane. The scattered wave vector $\mathbf{k}$ is defined by the polar angles θ and ϕ. The figure shows a double-scattering event within the cell. (x,y,z) in this figure, although in the same notation, obviously differs from the one in Fig. 1.

By looking at the form of the nth order term (15) we can can make an important observation that the scattering amplitude calculated for a particle situated at position $\bar{R}$ is simply related to the scattering amplitude calculated for a particle situated at the origin by a multiplicative factor $\exp(i\bar{q}\cdot\bar{R})$. Thus the scattering matrix for a particle situated at $\bar{R}$ is given in terms of the scattering matrix defined in Eq. (4) by

$$\bar{\bar{S}}(\bar{R}) = \bar{\bar{S}}\exp(i\bar{q}\cdot\bar{R}). \tag{24}$$

We also know that when the expansion (12) converges the scattering matrix can be written as

$$\bar{\bar{S}} = \sum_{n=0}^{\infty}\bar{\bar{S}}^{(n)}. \tag{25}$$

For example, by using Eqs. (18) and (19) we see that for the lowest order the polarized scattering amplitude is given by

$$S_1^{(1)} = \frac{i}{4\pi}k^3(m^2-1)\int_v d^3\rho'\exp(i\bar{q}\cdot\bar{\rho}')$$
$$S_2^{(1)} = -\cos\Theta S_1^{(1)}, \qquad S_3^{(1)} = S_4^{(1)} = 0 \tag{26}$$

B. Asano-Yamamoto Formalism for Scattering from a Spheroid

A rigorous solution of electromagnetic wave scattering from a spherical particle as a boundary value problem was achieved by Mie[11] in 1908, and the method is well described in Ref. 1. Due to symmetry of a sphere the scattering matrix $\bar{\bar{S}}(\Theta)$ is only a function of $\hat{k}\cdot\hat{k}'$ and is therefore time-independent. From the point of view of the dynamic light scattering, it is of little interest because the time dependence of the field correlation function comes entirely from the translational factor $\exp[i\bar{q}\cdot\bar{R}(t)]$, and as far as the time dependence is concerned it is equivalent to a point particle. On the other hand as soon as the shape of the particle deviates from sphericity a new vector $\hat{v}(t)$ comes into the picture, and the dynamic form factor becomes time-dependent. The light scattering spectrum thus reflects the rotational as well as the translational motions of the particle.

Extension of the Mie theory to a particle with a spheroidal geometry was done by Asano and Yamamoto (A-Y) in 1975, and details of the solution were described in Ref. 10. A-Y used a coordinate system as depicted in Fig. 2 where the $\hat{v}$ vector points always in the $\hat{z}$ direction. The incident wave vector $\hat{k}$ lies in x-z plane with an inclination angle ζ from the z axis. The scattered vector $\hat{k}'$ is in an arbitrary direction specified by polar angles (θ,ϕ). Although A-Y provides an exact solution to the scattering problem, in order for this formalism to be useful, we must relate the coordinate system used by A-Y (where $\hat{v}$ is fixed) to the coordinate system in our laboratory setup (where $\hat{k},\hat{k}'$, and $\hat{\epsilon}$ are fixed).

In the A-Y coordinates the scattered fields are related to the incident fields by

$$\begin{pmatrix} E_{\mathrm{TE}} \\ E_{\mathrm{TM}} \end{pmatrix} = \begin{pmatrix} T_{11} T_{21} \\ -T_{12} T_{22} \end{pmatrix} \begin{pmatrix} E_{\mathrm{OTE}} \\ E_{\mathrm{OTM}} \end{pmatrix} \frac{\exp(ikr)}{-ikr} \exp(-i\bar{k}\cdot\bar{r}), \tag{27}$$

where E_{TE} and E_{TM} are the TE and TM components, respectively, of the scattered field and likewise E_{OTE} and E_{OTM} that of the incident field. In order to relate the scattering matrix $\overline{\overline{T}}$ in Eq. (27) to that of $\overline{\overline{S}}$ in Eq. (16) we must express[12]

$$\begin{pmatrix} E_{\mathrm{OTE}} \\ E_{\mathrm{OTM}} \end{pmatrix} = \overline{\overline{A}} \begin{pmatrix} E_{ot} \\ E_{ol} \end{pmatrix}, \tag{28}$$

$$\begin{pmatrix} E_{\mathrm{TE}} \\ E_{\mathrm{TM}} \end{pmatrix} = \overline{\overline{B}} \begin{pmatrix} E_{st} \\ E_{sl} \end{pmatrix}, \tag{29}$$

where matrices $\overline{\overline{A}}$ and $\overline{\overline{B}}$ are functions of angles of ζ, θ, and ϕ, defined in Fig. 2. Then, from Eqs. (27) and (6) we obtain a relation

$$\overline{\overline{S}} = (\overline{\overline{B}})^{-1} \cdot \overline{\overline{T}} \cdot \overline{\overline{A}} \tag{30}$$

where

$$\overline{A} = \gamma^{-1/2} \begin{pmatrix} \cos\zeta \sin\theta \cos\phi - \sin\zeta \cos\theta & -\sin\theta \sin\phi \\ \sin\theta \sin\phi & \cos\zeta \sin\theta \cos\phi - \sin\zeta \cos\theta \end{pmatrix}, \tag{31}$$

$$(\overline{B})^{-1} = C\gamma^{-1/2} \begin{pmatrix} \sin\zeta \cos\theta \cos\phi - \cos\zeta \sin\theta & -\sin\zeta \sin\phi \\ \sin\zeta \sin\phi & \sin\zeta \cos\theta \cos\phi - \cos\zeta \sin\theta \end{pmatrix}, \tag{32}$$

$$\gamma = \cos^2\zeta \sin^2\theta + \sin^2\zeta \cos^2\theta \begin{matrix} -2 \sin\zeta \cos\zeta \cos\theta \sin\theta \cos\phi \\ + \sin^2\zeta \sin^2\theta \sin^2\phi \end{matrix}, \tag{33}$$

$$C = [\sin^2\zeta \sin^2\phi + (\sin\zeta \cos\theta \cos\phi - \cos\zeta \sin\phi)^2]^{-1}. \tag{34}$$

It is important to observe from Fig. 2 that for a symmetric body like a spheroid the scattering matrix $\overline{\overline{T}}$ in the body frame can depend only on the three angles (θ,ϕ,ζ). Therefore, the scattering matrix $\overline{\overline{S}}$ in the laboratory frame should also depend only on three angles, for example (θ_s,ϕ_s,Θ). For a case of less-symmetric body, $\overline{\overline{S}}$ in general depends on relative angles of all four vectors $\hat{V},\hat{k},\hat{k}'$, and $\hat{\epsilon}$.

C. Scattered Field Autocorrelation Function

Consider a volume element in the medium illuminated by the laser beam. It contains N identical spheroidal scattering centers (bacteria) making random motions. The scattered field can be expressed as

$$\overline{E}_s(t) = \begin{pmatrix} E_{st} \\ E_{sl} \end{pmatrix} = \sum_{i=1}^{N} \exp(i\bar{q}\cdot\overline{R}_i(t)) \begin{pmatrix} S_1 S_4 \\ S_3 S_2 \end{pmatrix} \begin{pmatrix} E_{ot} \\ E_{ol} \end{pmatrix} \frac{\exp(ikr)}{-ikr} \exp(-i\bar{k}\cdot\bar{r}). \tag{35}$$

Take $E_{ol} = 0$ as in Fig. 1, then the polarized component of the scattered field autocorrelation function is

$$\langle \overline{E}_s^*(0)\cdot\overline{E}_s(t)\rangle_P = \frac{|E_o|^2 \exp(-i\omega t)}{k^2 r^2} \times \left\langle \sum_{i=1}^{N}\sum_{j=1}^{N} \exp\{i\bar{q}\cdot[\overline{R}_j(t) - \overline{R}_i(0)]\} \cdot S_1^*[\hat{V}_i(0),\hat{k},\hat{k}',\hat{\epsilon}] S_1[\hat{V}_j(t),\hat{k},\hat{k}',\hat{\epsilon}] \right\rangle, \tag{36}$$

and the depolarized component of the scattered field autocorrelation function is

$$\langle \overline{E}_s^*(0)\cdot\overline{E}_s(t)\rangle_{DP} = \frac{|E_o|^2 \exp(-i\omega t)}{k^2 r^2} \times \left\langle \sum_{i=1}^{N}\sum_{j=1}^{N} \exp\{i\bar{q}\cdot[\overline{R}_j(t) - \overline{R}_i(0)]\} \cdot S_3^*[\hat{V}_i(0),\hat{k},\hat{k}',\hat{\epsilon}] S_3[\hat{V}_j(t),\hat{k},\hat{k}',\hat{\epsilon}] \right\rangle. \tag{37}$$

If the motion of particles is uncorrelated as in the case of the bacteria population, the $i \neq j$ terms in Eq. (36) and (37) give zero contribution, and we have simply

$$\langle \overline{E}_s^*(0)\cdot\overline{E}_s(t)\rangle_P = \frac{N|E_0|^2 \exp(-i\omega t)}{k^2 r^2} \times \langle \exp\{i\bar{q}\cdot[\overline{R}(t) - \overline{R}(0)]\} S_1^*(0) S_1(t)\rangle, \tag{38}$$

where $\overline{R}(t)$ is the center of mass coordinate of a typical particle at t. Similarly

$$\langle \overline{E}_s^*(0)\cdot\overline{E}_s(t)\rangle_{DP} = \frac{N|E_o|^2 \exp(-i\omega t)}{k^2 r^2} \times \langle \exp\{i\bar{q}\cdot[\overline{R}(t) - \overline{R}(0)]\} S_3^*(0) S_3(t)\rangle. \tag{39}$$

The bracket average in all equations shown above refers to two kinds of averages: namely, average over motions of the particles and average over their orientations or direction of motions.

In the photon correlation measurement what is usually measured is the so-called intermediate scattering function defined as

$$F_s(\bar{q},t) = \frac{\langle E_s^*(0)\cdot E_s(t)\rangle}{\langle |E_s(0)|^2\rangle}. \tag{40}$$

We shall calculate the intermediate scattering function for nonmotile and motile bacteria in the following sections.

D. Scattered Intensity

Both polarized and depolarized intensities follow from Eqs. (38) and (39) by setting $t = 0$. When we carry out the orientational average, the result is

$$\begin{bmatrix} I(\Theta)_P \\ I(\Theta)_{DP} \end{bmatrix} = \frac{N|E_0|^2}{4\pi k^2 r^2} \int_0^{2\pi} d\phi_s \int_0^{\pi} d\theta_s \sin\theta_s \begin{bmatrix} |S_1(\theta_s,\phi_s,\Theta)|^2 \\ |S_3(\theta_s,\phi_s,\Theta)|^2 \end{bmatrix}. \tag{41}$$

It is seen that the scattered intensity is independent of the state of motions of particles provided that their directions of motion are random and isotropic.

E. Correlation Function for a Diffusing Particle[7]

This corresponds to a case when the bacteria are nonmotile and can be treated as Brownian particles in suspension. We have shown[6,7] that for a micron size particle, only the translational diffusion contribution is important, and in the time scale of interest the time dependence of $\hat{V}(t)$ can be neglected. Thus the motional average of the translational factor gives

$$\langle \exp\{i\bar{q}\cdot[\overline{R}(t) - \overline{R}(0)]\}\rangle = \exp\left(-\frac{\chi}{\beta} + \frac{\chi}{3} - \chi\mu^2\right), \tag{42}$$

where the scaled time variable

$$\chi = \overline{D} q^2 \beta t \tag{43}$$

depends on the average translational diffusion constant $D = (D_\parallel + 2D_\perp)/3$ and the eccentricity $\beta = (D_\parallel - D_\perp)/\bar{D}$ of a spheroid,[7] and

$$\mu \equiv \hat{q} \cdot \hat{V} = \sin\theta_s[-\cos\phi_s \sin\Theta + \sin\phi_s(1 - \cos\Theta)]/[2(1 - \cos\Theta)]^{1/2}. \quad (44)$$

The orientationally averaged intermediate scattering function is thus

$$\begin{bmatrix} F_s(\bar{q},t)_P \\ F_s(\bar{q},t)_{DP} \end{bmatrix} = \exp\left(-\frac{\chi}{\beta}\right) \exp\left(\frac{\chi}{3}\right) x[''']$$

$$[''] = \frac{\int_0^{2\pi} d\phi_s \int_0^{\pi} d\theta_s \sin\theta_s \begin{bmatrix} |S_1(\theta_s,\phi_s,\Theta)|^2 \\ |S_3(\theta_s,\phi_s,\Theta)|^2 \end{bmatrix} \exp[-\chi\mu^2(\theta_s,\phi_s,\Theta)]}{\int_0^{2\pi} d\phi_s \int_0^{\pi} d\theta_s \sin\theta_s \begin{bmatrix} S_1(\theta_s,\phi_s,\Theta)^2 \\ S_3(\theta_s,\phi_s,\Theta)^2 \end{bmatrix}}. \quad (45)$$

F. Correlation Function for a Freely Translating Particle[7]

This corresponds to a case when the bacteria move along straight lines for distances much longer than q^{-1}. Furthermore, their motions are isotropic with a Maxwellian speed distribution.[13] Again, there is no time dependence for $\hat{V}(t)$, and the motional average was shown to be[6]

$$\langle \exp\{i\bar{q} \cdot [\bar{R}(t) - \bar{R}(0)]\} \rangle = (1 - 2W^2\mu^2) \exp(-W^2\mu^2), \quad (46)$$

where the scaled time variable

$$W = qt(\langle V^2 \rangle/6)^{1/2}, \quad (47)$$

and $\langle V^2 \rangle$ is the rms speed of the Maxwellian distribution. The orientationally averaged intermediate scattering function is therefore

$$\begin{bmatrix} F_s(\bar{q},t)_P \\ F_s(\bar{q},t)_{DP} \end{bmatrix} = \frac{\int_0^{2\pi} d\phi_s \int_0^{\pi} d\theta_s \sin\theta_s \begin{bmatrix} |S_1(\theta_s,\phi_s,\Theta)|^2 \\ |S_3(\theta_s,\phi_s,\Theta)|^2 \end{bmatrix} \exp(-W^2\mu^2)(1 - 2W^2\mu^2)}{\int_0^{2\pi} d\phi_s \int_0^{\pi} d\theta_s \sin\theta_s \begin{bmatrix} |S_1(\theta_s,\phi_s,\Theta)|^2 \\ |S_3(\theta_s,\phi_s,\Theta)|^2 \end{bmatrix}}. \quad (48)$$

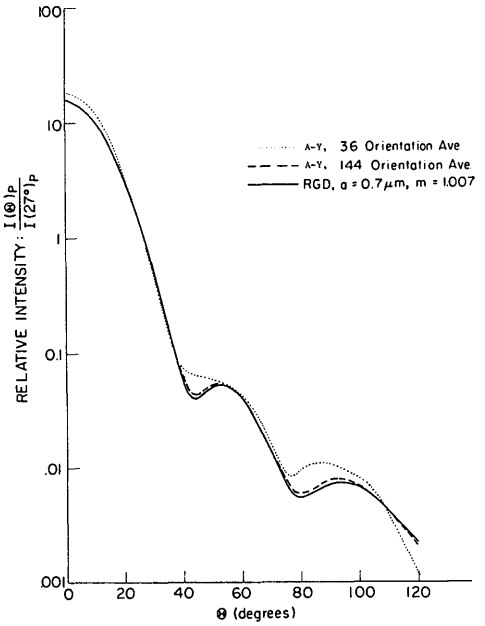

Fig. 3. Relative scattering intensity vs scattering angle for polarized radiation: $a = 0.7\ \mu m$; $a/b = 1.944$; $m = 1.007$. This figure shows the effect of increasing the number of orientations of the spheroid used in averaging the scattered intensity over a randomly oriented ensemble of cells. The RGD approximation is calculated with completely random orientations.

III. Computation

The computer code for calculating the A-Y scattering amplitude T_{ij} in Eq. (27) was developed by Asano.[10,14] We developed subroutines which transform $\bar{\bar{T}}$ to $\bar{\bar{S}}$ matrix and then compute the intensity and intermediate scattering function. The code was written in Fortran, and it was run with an IBM 360/95 computer at the NASA Goddard Institute for Space Studies.[15] An average run time for a set of size parameters is about 2–6 min. The result contains all data for the intensities and correlation functions at 40 scattering angles ranging from $\Theta = 3°$ to 120°.

The orientational average indicated in Eqs. (41), (45), and (48) are computed in the following sequence:

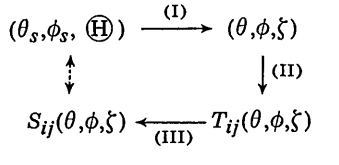

At a given scattering angle Θ, we start by picking an orientation $\hat{V}$ of the spheroid in the laboratory frame by specifying angles (θ_s,ϕ_s). A transformation [step (I)] is then applied to find equivalent body frame angles (θ,ϕ,ζ):

$$\text{(I)} \begin{cases} \cos\zeta = \sin\theta_s \sin\phi_s \\ \cos\theta = \sin\theta_s(\cos\phi_s \sin\Theta + \sin\phi_s \cos\Theta) \\ \cos\phi = [\cos\Theta - \sin^2\theta_s \sin\phi_s(\cos\phi_s \sin\Theta + \sin\phi_s \cos\Theta)]/D \\ D = \{(1 - \sin^2\theta_s \sin^2\phi_s)[1 - \sin^2\theta_s(\cos\phi_s \sin\Theta + \sin\phi_s \cos\Theta)^2]\}^{1/2}. \end{cases}$$

From this set of body frame angles we then calculate $T_{ij}(\theta,\phi,\zeta)$ by using Asano's code [step (II)]. Finally we transform T_{ij} to S_{ij} by using transformation matrices $\bar{\bar{A}}$ and $(\bar{\bar{B}})^{-1}$ given in Eqs. (31) and (32) [step (III)]. With this S_{ij} so obtained we then calculate all quantities of interest for this orientation multiplying with a weighting factor $\sin\theta_s \Delta\theta_s \Delta\phi_s$. We then go to a next orientation $(\theta_s + \Delta\theta_s, \phi_s + \Delta\phi_s)$ and repeat the process. Three sets of orientational averages were tried: they are 36, 144, and 324 orientations, respectively.

IV. Results and Discussion

A. Scattered Intensity Distribution

For a homogeneous bacteria sample angular dependence of the scattering intensity can be used to fix a set of size parameters such as a, b, and the relative index of refraction m,[7] assuming the bacterium can be represented by a homogeneous solid spheroid. It is therefore an essential first step before understanding of the dynamic light scattering spectra can be attempted. For the convenience of displaying measurements we usually normalize the measured intensity at an angle Θ by that of $\Theta = 27°$. This relative intensity contains only the essential angular dependence of the scattering matrix $|S_{ij}|^2$ (in the case of A-Y scattering) or the form factor $|a_1(q,\mu)|^2$ (in the case of RGD scattering).

Figure 3 shows the angular dependence of the relative polarized scattered intensity. The solid line refers to the orientationally averaged RGD approximation calculated according to[7]

$$\frac{I(\Theta)_{RG}}{I(27°)_{RG}} = \frac{\int_{-1}^{1} d\mu |a_1(\bar{q},\mu)|^2,}{\int_{-1}^{1} d\mu |a_1(\bar{q}_0,\mu)|^2}, \tag{49}$$

where $q_0 = 2k \sin(27°/2)$, and $a_1(q,\mu)$ is given in Eq. (20). The A-Y scattering intensity is calculated according to Eq. (41). The orientational average is done as described in Sec. III. In order to test the number of orientations needed to achieve a full orientational average, we first pick 36 orientations uniformly over a sphere. This gives a result shown by the dotted line. Next, we increase the number of orientations over the sphere to 144, and we get a result shown by the dashed line. A further increase in number of orientations (324) does not change the result significantly. Thus we establish a criterion that 144 orientations are needed to achieve a good orientational average for the intensity calculations. We, therefore, in all subsequent intensity calculations, adopt 144 orientations as a sufficient average. As we can see from comparison of the dashed line and the solid line that the RGD approximation is excellent for the case $a = 0.7$ μm, $a/b = 1.944$, and $m = 1.007$. We notice that while the A-Y scattering depends both on the size parameters a and b and the relative index of refraction m, the RGD does not depend on m. Nevertheless we know that RGD is valid only when $|m - 1| \ll 1$.

Figure 4 shows an effect of increasing m with the size parameters kept fixed. At $m = 1.03$ we see that a larger discrepancy occurs at $\Theta = 90°$, and the RGD is in error as much as 28% while the corresponding error for the case $m = 1.007$ is only 9% (see Fig. 3). Also the intensity minima predicted by RGD are slightly shifted from the correct values.

Figure 5 shows an effect of increase the size parameter a to 0.9 μm, while m is kept at 1.007. The worst discrepancy also occurs at 90°, but it is no more than 10%.

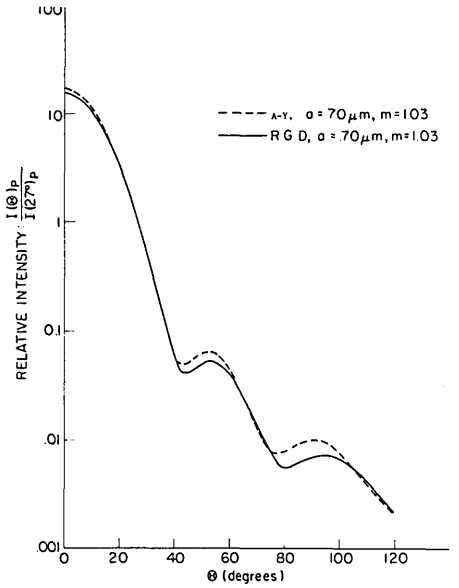

Fig. 4. Relative scattering intensity vs scattering angle for polarized radiation: $a = 0.7$ μm; $a/b = 1.944$; $m = 1.03$. The figure shows deviation of the RGD approximation from the A-Y theory for a relatively large m.

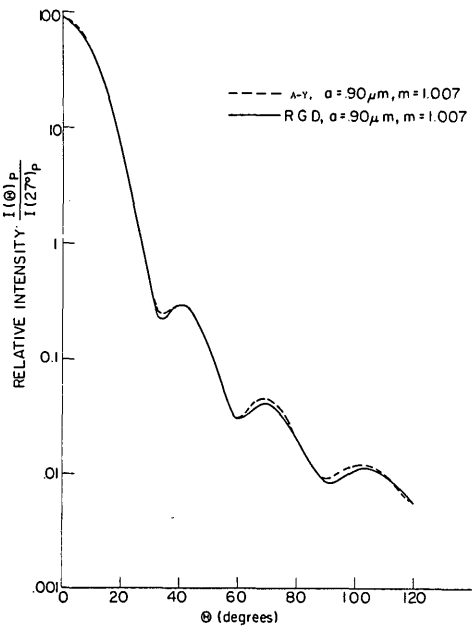

Fig. 5. Relative scattering intensity vs scattering angle for polarized radiation: $a = 0.9$ μm; $a/b = 1.944$; $m = 1.007$. The figure shows effects of increasing the size of parameter a to 0.90 μm.

Figure 6 shows a relative intensity of the depolarized to the polarized components, calculated by the A-Y theory for the standard parameters with Eq. (41). In RGD this ratio is zero while in the A-Y theory this is no more than 10^{-5} and is insignificant.

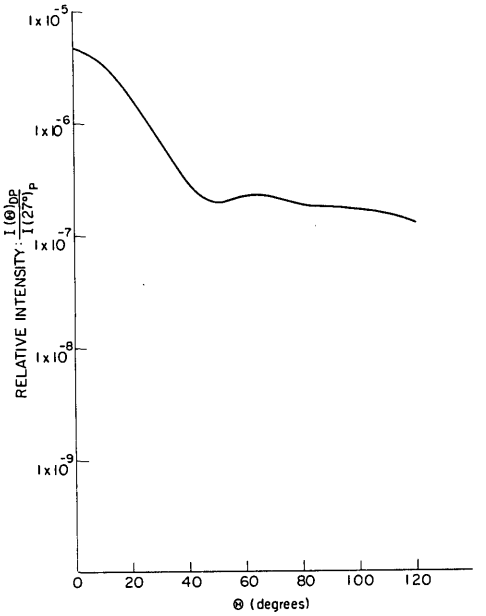

Fig. 6. Relative depolarized scattering intensity vs scattering angle for a case: $a = 0.7\ \mu$m; $a/b = 1.944$; $m = 1.007$, calculated based on the A-Y theory. In the RGD approximation the depolarized component of the scattered intensity is zero. This figure shows that the depolarized scattered intensity is very small compared with the polarized component at all angles.

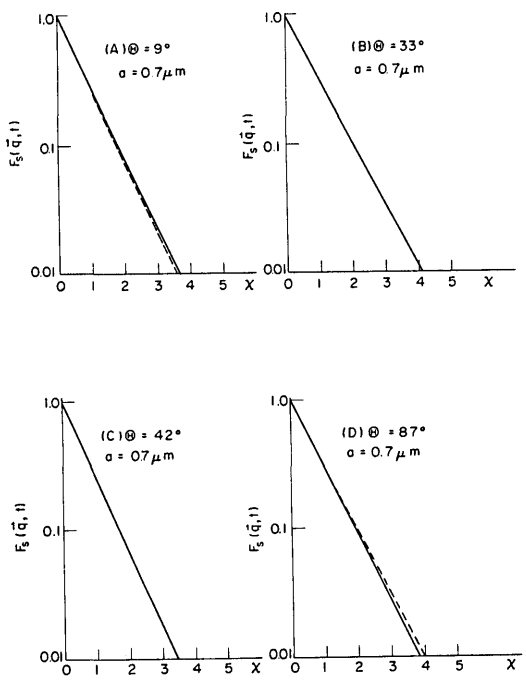

Fig. 7. Intermediate scattering function vs $\chi \equiv \overline{D}q^2\epsilon t$ for a diffusing cell. The cell size is $a = 0.7\ \mu$m, $a/b = 1.944$: (A) — RGD and A-Y (144 orientations) for $m = 1.007$ and $m = 1.03$, --- A-Y (36 orientations) for $m = 1.007$; (B) RGD and A-Y (144 orientations) for $m = 1.007$ and $m = 1.03$; (C) RGD and A-Y (144 orientations) for $m = 1.007$ and $m = 1.03$; (D) — RGD and A-Y (144 orientations) for $m = 1.007$, --- A-Y (144 orientations) for $m = 1.03$.

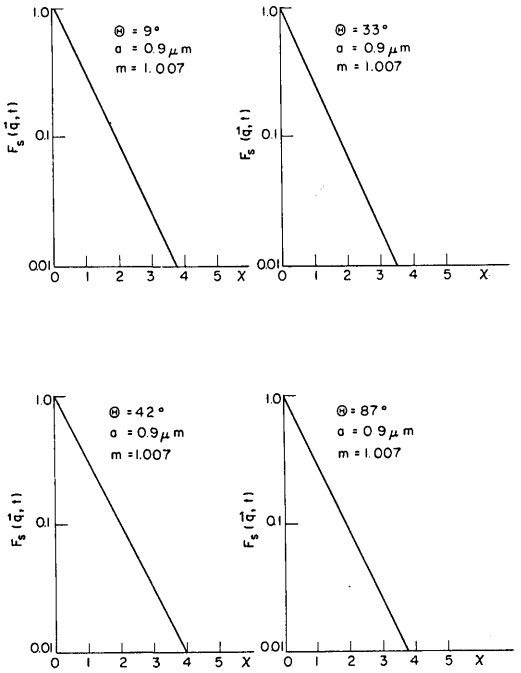

Fig. 8. Intermediate scattering function vs χ for a diffusing cell. RGD and A-Y (144 orientations) for a larger cell size: $a = 0.9\ \mu$m; $a/b = 1.944$.

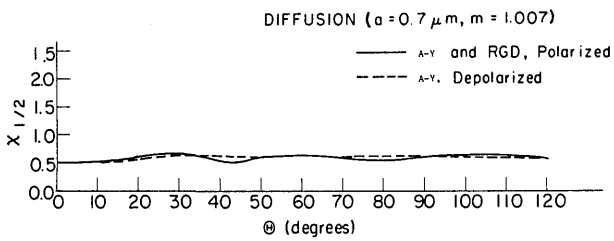

Fig. 9. Halfwidth of the intermediate scattering function vs scattering angle for a diffusing cell.

B. Correlation Function for Nonmotile Bacteria

In RGD the intermediate scattering function was shown[7] to be

$$F_s(\overline{q},t) = \exp\left(-\frac{\chi}{\beta}\right)\exp\left(\frac{\chi}{3}\right)\frac{\int_{-1}^{1} d\mu\,|a_1(\overline{q},\mu)|^2\exp(-\chi\mu^2)}{\int_{-1}^{1} d\mu\,|a_1(\overline{q},\mu)|^2}, \quad (50)$$

which is independent of m. This is to be compared with the rigorous result (45).

In Fig. 7 we plot $F_s(\overline{q},t)$ as a function of the reduced time variable χ defined in Eq. (43). Figure 7(A) illustrates sensitivity to the orientational average of the A-Y calculation (45). We establish that 144 orientations are necessary to achieve a full average. Thus all subsequent calculations use this number of averages. Sensitivity to variation in m is also studied. For $a = 0.7\ \mu$m and $a/b = 1.944$, RGD results are indistinguishable from

the A-Y calculations except at Θ = 87° [Fig. 7(D)]. Even at this angle the halfwidth of the correlation function is practically the same in the two calculations. Figure 8 displays results of sensitivity study of size variation. We see that up to $a = 0.9\ \mu$m RGD is an excellent approximation. Figure 9 plots halfwidth of the correlation functions as a function of scattering angle for both polarized and depolarized scatterings. We see a striking similarity between $\chi_{1/2}$ for both the polarized and depolarized scatterings.

C. Correlation Function for Motile Bacteria

In RGD the intermediate scattering function was shown[7] to be

$$F_s(\bar{q},t) = \frac{\int_{-1}^{1} d\mu |a_1(\bar{q},\mu)|^2 (1 - 2W^2\mu^2) \exp(-W^2\mu^2)}{\int_{-1}^{1} d\mu |a_1(\bar{q},\mu)|^2}, \quad (51)$$

where the reduced time variable W was given in Eq. (47). This is again to be compared with the rigorous result (48). In Fig. 10 plots of $F_s(\bar{q},t)$ vs the reduced variable W are shown. Figures 10(A) and 10(B) indicate that in the case of free motions, 324 orientations are necessary to achieve a complete orientational average in the A-Y scattering, and we use this criterion for all subsequent calculations. We vary both the size parameters and m in Figs. 10 and 11. We observe some discrepancy between the A-Y calculations and RGD in the tail part of the correlation functions. However, as far as the halfwidths are concerned RGD approximation is reliable at all scattering angles for $m = 1.007$, but some discrepancy is observable at large scattering angles for $m = 1.03$ case. Figure 12 summarizes these results by plotting halfwidths of the correlation function as a function of scattering angles. Oscillations in $W_{1/2}$ vs Θ plot for motile bacteria *E. coli* has already been observed in experiments.[7] It is interesting to note that similar oscillations exist in the depolarized part of the scattering.

V. Conclusion

We have formulated a general procedure by which the scattered field amplitude correlation function, both polarized and depolarized contributions, can be computed for a collection of particles, once the one particle scattering matrix T_{ij} are given. These formula are displayed explicitly in Eqs. (36) and (37), and the transformation matrices to go from T_{ij} to S_{ij} are given in Eqs. (30), (31), and (32). We have given an explicit formula for the scattered intensity, both polarized and depolarized, for a collection of randomly diffusing or moving particles. Two specific cases for the intermediate scattering functions are worked out in detail: diffusing particles and freely moving particles with a Maxwellian speed distribution. We have then applied the formalism to microorganisms suspended in a liquid medium.

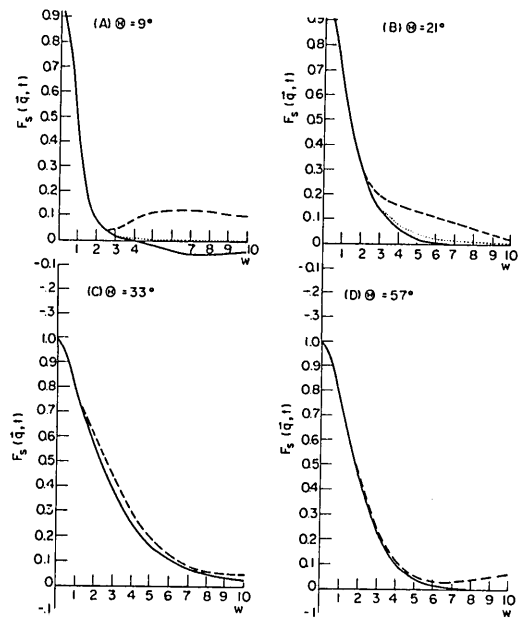

Fig. 10. Intermediate scattering functions vs $W \equiv qt(\langle v^2 \rangle/6)^{1/2}$ for motile cells: $a = 0.7\ \mu$m; $a/b = 1.944$; $m = 1.007$. ····· RGD (random orientations); --- A-Y (144 orientations); — A-Y (324 orientations).

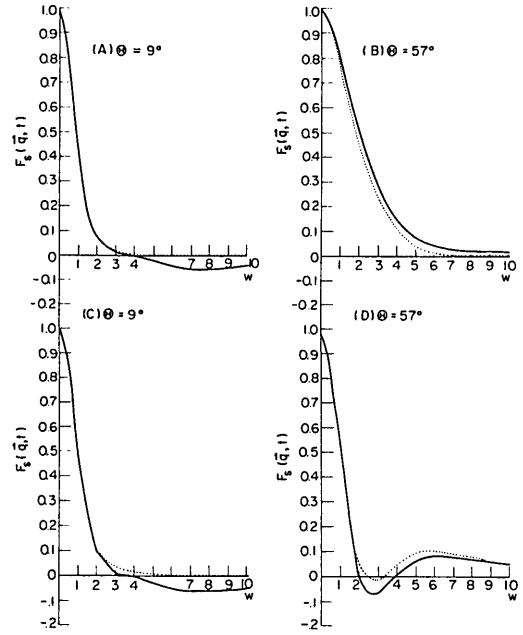

Fig. 11. Intermediate scattering function vs W for motile cells: ····· RGD (random orientations); — A-Y (324 orientations). (A),(B) $a = 0.7\ \mu$m, $a/b = 1.944$, $m = 1.03$; (C),(D) $a = 0.90\ \mu$m, $a/b = 1.944$, $m = 1.007$.

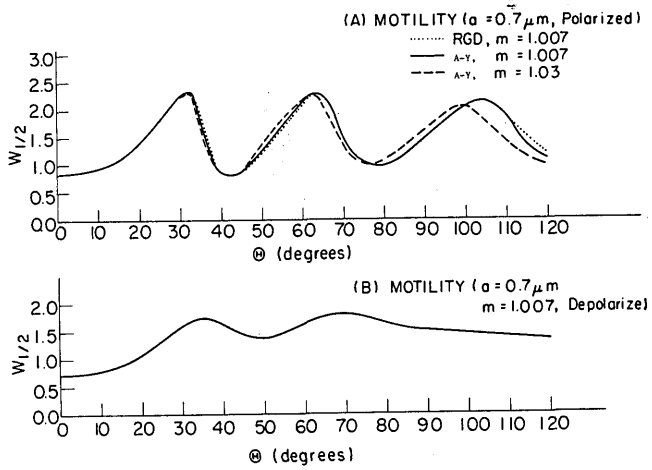

Fig. 12. Halfwidth of the intermediate scattering function vs scattering angle for motile cells.

In the case of *E. coli* where the approximate size parameters and the relative index of refraction m are known, we made a model calculation by assuming it to be a spheroid with semimajor and minor axes $a = 0.70$ μm, $a/b = 1.944$, and $m = 1.007$. Although this model is too simple to account for all the light scattering properties of *E. coli*,[6,7] nevertheless it should be good enough to test the validity of the RGD approximation. We calculated the scattered intensity as a function of scattering angle and show that the maximum deviation of RGD occurs at about $\Theta = 90°$, and it amounts to about 10% error. The depolarized contribution is shown to be completely negligible. The intermediate scattering functions for both nonmotile and motile cases are calculated. As far as the halfwidths vs scattering angles are concerned, RGD is certainly accurate to better than 10%. This assessment renders the approach taken in Refs. 6 and 7 meaningful because it shows that, within 10% accuracy, one can learn about the detailed motions of *E. coli* in suspension with a consistent use of the RGD approximation. In this paper we limit ourselves to studies of relatively simpler cases where the orientation vector $\hat{V}$ is time independent. Even in these cases interesting dependence of the halfwidth of the correlation functions vs the scattering angle can be observed. This dependence is absent in the case of spherical particles. A more realistic case is to consider time dependence of $\hat{V}(t)$ due to the rotational motion and its coupling to the translational motions. One such study was made in Ref. 9 with the RGD approximation.

We also made sensitivity studies of the results to variations in the size parameters a, b, and the relative index of refraction m. We show that for $m > 1.03$, RGD could be in serious error in computing the intensity as well as correlation functions. However, at $m = 1.007$, for sizes up to $a = 0.9$ μm and $a/b - 1.944$, the RGD seems to be still quite accurate. We suspect that RGD will gradually break down as the size of particle becomes larger than a micron even if we take $m = 1.007$ to be applicable to all microorganisms. Thus one has to be quite cautious in applying the RGD to other micron-size microorganisms, especially when m is known to be higher than 1.007.

This work was supported by the Sloan Fund for Basic Research of MIT and by the National Science Foundation. During the course of this study Shoji Asano held an NRC Resident Research Associateship supported by NASA; he was on leave from the Geophysical Institute of Tohoku University, Japan.

All reprint requests should be addressed to Sow-Hsin Chen at MIT.

References

1. H. C. van de Hulst, *Light Scattering by Small Particles* (Wiley, New York, 1957).
2. M. Kerker, *The Scattering of Light and Other Electromagnetic Radiation* (Academic, New York, 1969).
3. P. J. Wyatt, in *Methods in Microbiology, Vol. 8*, J. R. Norris and D. W. Ribbons, Eds. (Academic, New York, 1973).
4. R. Nossal, S.-H. Chen, and C. C. Lai, Opt. Commun. **4**, 35 (1971).
5. See a recent review of H. Z. Cummins, "Intensity Fluctuation Spectroscopy of Motile Micro-organisms," in *Photon Correlation Spectroscopy and Velocimetry*, H. Z. Cummins and E. R. Pike, Eds. (Plenum, New York, 1977), p. 200.
6. S.-H. Chen, M. Holz, and P. Tartaglia, Appl. Opt. **16**, 187 (1977).
7. M. Holz and S.-H. Chen, Appl. Opt. **17**, 1930 (1978).
8. M. Holz and S.-H. Chen, Appl. Opt. **17**, 3197 (1978).
9. M. Holz and S.-H. Chen, Biophys. J. **23**, 15 (1978).
10. S. Asano and G. Yamamoto, Appl. Opt. **14**, 29 (1975).
11. G. Mie, Ann. Phys. **25**, 377 (1908).
12. See Michael Kotlarchyk, "Light Scattering from Cells," M.S. Thesis, Massachusetts Institute of Technology (1978).
13. M. Holz and S.-H. Chen, Opt. Lett. **2**, 109 (1978).
14. S. Asano, Appl. Opt. **18**, 712 (1979), where an extensive calculation based on the code was made.
15. We are grateful to the Goddard Institute for Space Studies for use of its computer.